


# Incremental Optical Encoder Based on a Sinusoidal Transmissive Pattern

Chi-Hung Lee , Hsin-Jung Huang, Jui-Ping Chang, and Yi-Cheng Chen

**Abstract**—In this paper, a high-precision rotary encoder based on a sinusoidal transmissive pattern (STP) is proposed for detecting shaft rotation. The STP disk can be realized by coating bell-shaped transmissive area on a transparent glass. We optimize the STP design shape and parameters to achieve sinusoidal transmissive characteristics. The STP-based encoder consists of a light-emitting diode, a STP disk, and a photodetector array. Experimentally, the produced STP disk had a diameter of 60 mm. 256 columns of STPs were arranged on the circumference of this disk to provide a detection pitch of  $1.40625^\circ$ . Each column consisted of 50 bell-shaped STPs. In principle, an incident beam from a blue-ray light emitting diode illuminates the STP of the disk, and the angle of rotation is decoded from the sinusoidal distribution of transmissive spots on the PD. Compared with a conventional incremental rotary encoder, the proposed STP-based encoder achieves a superior angular resolution.

**Index Terms**—Disk, encoder, incremental, rotation, sinusoidal.

## I. INTRODUCTION

ROTARY encoders are key components in the monitoring of the rotation of mechanical parts [1] or the track steering angle [2], [3]. Optical encoders have a high resolution and allow for facile signal processing. Accurate optical encoders can be categorized into geometric, diffractive, interferometric, polarization, and ratiometric encoders.

Geometric encoders [4], [5] are suitable for detecting coarse angular resolutions. They generally comprise a circular disk that contains patterns of transparent and opaque areas, a light-emitting diode (LED) that emits light that passes through the transparent areas as the disk rotates, and an optical detector that senses when a transparent area passes in front of it. Diffractive encoders [6]–[8] have a similar design to geometric optical encoders. Diffractive encoders use a collimated laser beam to illuminate a reflective microstructured plastic disk. The reflected and diffracted beam propagate to an array of photodetectors (PDs) placed at different first-order deflection angles, which enables diffractive encoders to determine the rotation angle of

the disk. Interferometric encoders [9], [10] are expensive but can achieve subnanometer resolution. They usually follow the laser interference principle for fine-pitch gratings. The collimated beam first illuminates a fixed scale grating. Then, the first two reflected and diffracted beams interfere to form fringes. Finally, signal processing of the fringes provides the displacement of the fixed scale (or disk). Polarization encoders [11] consist of an LED, a rotating disk made of an aluminum nanowire-grid linear polarizer, a pair of stationary linear polarizers, and a PD array. During operation, the received signal intensities from the PD array are orthogonally polarized. Their differential value depends on the rotation angle of the disk. In ratiometric encoders [12], a collimated beam is propagated onto a spirally coated rotary encoder at an angle of  $45^\circ$ . The ratio of transmitted to reflected intensities is used to determine the rotation angle.

Diffractive, interferometric, and ratiometric encoders are light, compact, and accurate. These encoders have a complex design, and several of their parts must be assembled precisely. By contrast, geometric encoders have a simple design for signal processing and thus are widely used. In this paper, we introduce the sinusoidal transmissive pattern (STP) encoder, which is a geometric encoder that can detect the rotation angle of a shaft. The main concept is derived from the studies of Tahereh [12] and Mayer [6]. This concept is verified through various experiments in the present study. The STP encoder exhibits similar features to conventional geometric encoders but is smaller. This study implemented the STP encoder and characterized it on the basis of the experimental results. The rest of this paper is organized as follows. Section II describes the operation principle of the rotary encoder and the design methodology. Section III presents a discussion on the fabrication, measurement results, and analysis of the STP encoder. Finally, section IV presents the conclusion.

## II. DESIGN AND SIMULATION

The design concept is derived from several prior studies. A conventional incremental rotary encoder consists of a source, a collimator lens, an index grating, a scale grating, and a PD. As shown in Fig. 1a, the optical system is designed to generate a sawtooth signal received by a single PD, which can be achieved by having a collimated beam passing through a fixed rectangular index grating and moveable rectangular scale grating. For more accurate detection, the optical system (Fig. 1b) can be adjusted to generate a sinusoidal signal and use phase-quadrature interpolation, which is achieved by designing an index grating and a scale grating with a small pitch difference. To reduce

Manuscript received July 26, 2021; revised October 26, 2021; accepted November 17, 2021. Date of publication November 23, 2021; date of current version December 9, 2021. This work was supported in part by Industrial Technology Research Institute, Taiwan. The Development of Key Technologies for Industrial Sensors (4/4):109-EC-17-A-24-1441. (Corresponding author: Chi-Hung Lee.)

Chi-Hung Lee is with the Department of Electrical Engineering, Feng-Chia University, Taichung 40724, Taiwan (e-mail: tainanncku@hotmail.com).

Hsin-Jung Huang, Jui-Ping Chang, and Yi-Cheng Chen are with the Smart Microsystems Technology Center, Industrial Technology Research Institute, Tainan 709, Taiwan (e-mail: p1897104@itri.org.tw; qqruei@itri.org.tw; ben\_son\_chen@itri.org.tw).

Digital Object Identifier 10.1109/JPHOT.2021.3129820

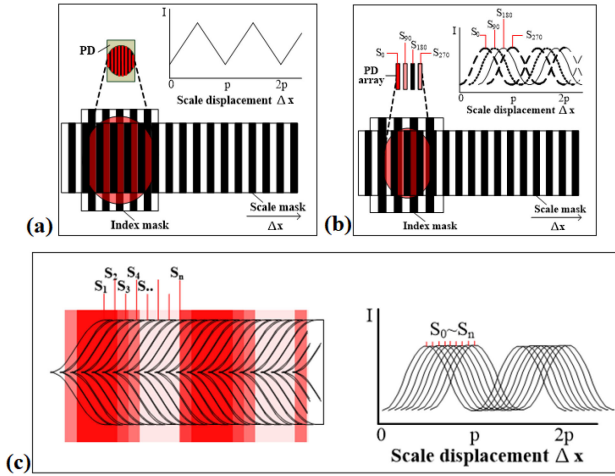


Fig. 1. (a) Imaging Moire encoder and its output triangular signal; (b) Optical encoder with an index grating and a scale grating with a small pitch difference. (c) IC-HAUS' reflective encoder that uses a curved PD array to transform an incident trapezoidal image into a sequence of sinusoidal signals.

the number of components and improve the performance of the encoder, Jason [13] invented an encoder apparatus including a scale grating and a readhead. The readhead consists of an array of PD elements for detecting a scale signal falling on the sensor. By adjusting the length of each PD according to a window function, the output signal is ensured to have a limited adverse effect on the undesirable frequencies from the scale grating signal to reduce the subdivisional error of the encoder. Another method is adopted by a commercial reflective encoder provided by iC-HAUS [14]. The encoder's readhead consists of a curved PD array (Fig. 1c) that detects a trapezoidal signal and outputs it to a sequence of phase-shift sinusoidal signals as the scale grating moves. These prior studies show that the final output signals consist of at least two sinusoidal signals—the quadrature SIN and COS signals—for determining the position of the scale grating.

#### A. STP Disk

To generate a sinusoidal signal without using an index gating, STP adopts a bell-shaped transmissive area to generate the sinusoidal signal directly. Another potential shape is the sinusoidal gray-level pattern. However, to generate patterns of sinusoidal transmittance along the circumference of the disk, it requires laser direct writer to make the gray-level pattern [15], which is expensive. Our method is based on coding binary pattern, which is similar to design a gray-tone mask composed of bars and apertures [16]. The pattern layout of STP is displayed in Fig. 2a. This layout possesses a stepwise form to produce a Gaussian-like transmissive area of which a cross-sectional view is shown in the graph of Fig. 2b.

The stepwise form of fabricated STP is a discrete form of the ideal STP. There are 50 STPs along the radial direction. Each STP is composed of 45 portions along the circumferential direction. The portion has a width of  $12 \mu\text{m}$ . Compared with the ideal STP, the maximum length difference along the radial

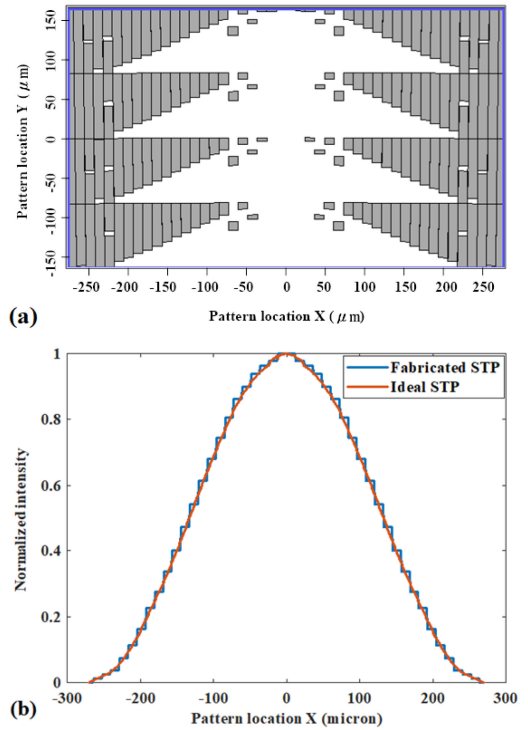


Fig. 2. (a) Pattern layout used to produce a sinusoidal transmissive area; (b) Cut through the transmitted intensity distribution obtained from the pattern layout.

direction between the fabricated STP and the ideal STP is  $10.3 \mu\text{m}$ . For each group of the four light-receiving portions ( $S_0, S_{90}, S_{180},$  and  $S_{270}$ ), the induced intensity error can be calculated from the summation difference of the transmissive area between the fabricated STP and that of the ideal STP. The maximum induced difference is 0.237%.

The working principle of STP encoder is based on the interaction of an illumination spot with STPs on the encoder disk. A simple incremental code disk consists of a sequence of STPs on the circumference of the encoder disk (Fig. 3a). When the encoder disk is rotated relative to the illumination, this alternating sequence allows light to transmit sinusoidally. This process is similar to a single track of a conventional binary code. The major difference is that the pattern composition of STP can generate sinusoidal signal directly (Fig. 3b). The spatial sinusoidal power can be analyzed to obtain information on the angular position. In our model, a PD array (four-phase quadrature detectors) was used to detect the spatial distribution of transmitted power without the usage of collimation optics.

#### B. System Design

For a rotary sensor, a sinusoidal signal can be interpolated to achieve a high angular resolution. Because the signal is a product of the interaction between the illumination and the STP, an interaction model must be developed. As displayed in Fig. 4a and 4b, each constituent parameter is defined as follows. Let  $g_1$  ( $= g$ ) be the distance between the LED source and the disk surface,  $g_2$  ( $= g$ ) be the distance between the disk surface and the PD array,  $p_1$  be the pitch of the STP on the disk, and  $p_2$  be the

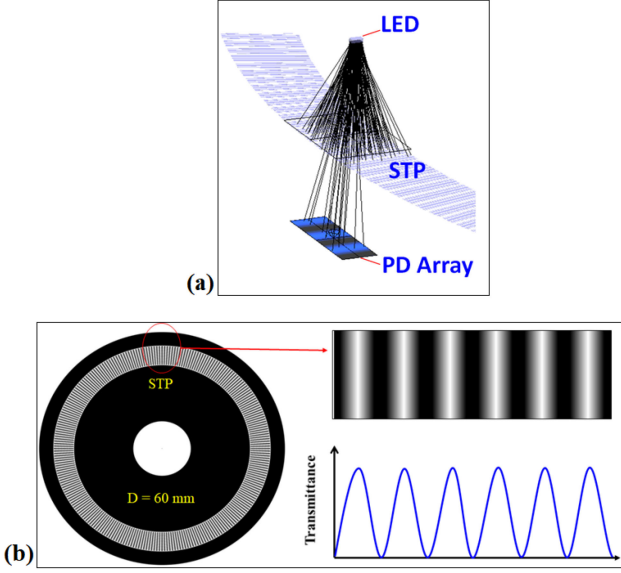


Fig. 3. (a) Optical path of the STP-based optical encoder; (b) Sequence of the STP on the circumference of an aluminum-coated encoder disk. Periodic sinusoidal transmissive area can generate a periodical signal directly.

pitch of the bright-and-dark pattern projected on the PD array. The pattern pitch  $p_2$  can be calculated by using (1):

$$p_2 = \frac{g_1 + g_2}{g_2} p_1 = h p_1 \quad (1)$$

The location of the LED is  $(0, R, g_1)$ , where  $R$  is the radial distance from the disk center.  $\theta$  is the angle between  $y$ -axis and the line joining the disk center and each STP. If a ray from the LED is intercepted by the STP at  $(R \sin \theta, R \cos \theta, 0)$ , it projects onto the PD array at point P:

$$P : (h \times R \sin \theta, h \times (R \times \cos \theta - 1) + R, -g_2) \quad (2)$$

Fig. 4c is an enlarged plan view of the PD area. The PD array includes a light-receiving group having one-dimensionally arranged light-receiving portions. The light-receiving portions are divided into four groups:  $S_0$ ,  $S_{90}$ ,  $S_{180}$ , and  $S_{270}$ . These groups are electrically connected at period  $p_2$  to detect four phase portions of a bright-and-dark pattern with period  $p_2$  that are  $90^\circ$  out of phase with each other. For example,  $S_0$  and  $S_{180}$  are signals that are  $180^\circ$  out of phase with each other. Let us consider an optical encoder for rotation measurement in which the final electrical signals are two sinusoids shifted by  $90^\circ$ :  $S_A (= S_0 - S_{180})$  and  $S_B (= S_{90} - S_{270})$ . With these two signals, the relative rotation within  $p_1$  produced between the scale and the readhead can be easily determined using the arctangent algorithm [17]. The phase  $\Phi_{A,B}$  derived from signals  $S_A$  and  $S_B$  is used to interpolate the angle between two consecutive STPs, which are equivalent to each other. The phase  $\Phi_{A,B}$  can be calculated by using (3) [18]:

$$\Phi_{A,B} = \begin{cases} -0.5 + \tan^{-1} \left( \frac{S_B}{S_A} \right) / \pi & \text{if } S_A > 0 \\ +0.5 + \tan^{-1} \left( \frac{S_B}{S_A} \right) / \pi & \text{if } S_A < 0 \end{cases} \quad (3)$$

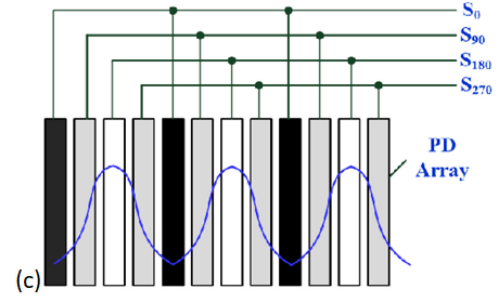
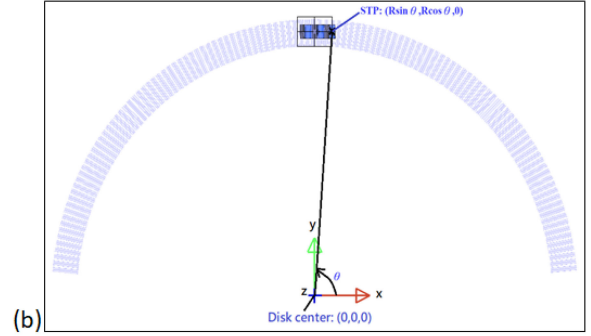
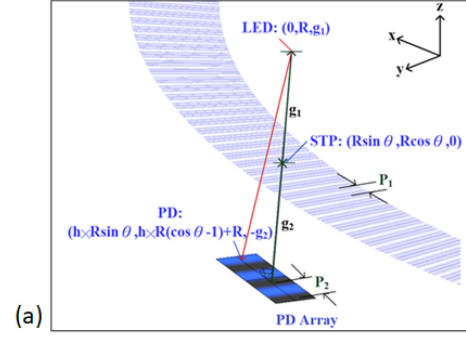


Fig. 4. (a) Side-view and (b) top-view of the design parameters for the STP-based optical encoder; (c) Enlarged view of the PD array.

### C. Simulation

Ray optic simulations were conducted to determine the structural parameters associated with its optical performance. The outcome of the design is shown in Fig. 5a. The light source comprises a  $90 \times 180\text{-}\mu\text{m}^2$  blue LED chip operating at  $\lambda = 470\text{ nm}$ . The STP disk contains an STP with a pitch of  $688\text{ }\mu\text{m}$  on a thin glass disk with a radius of  $30\text{ mm}$ , a resolution of 256 increments has been designed. The LED illuminated the STP disk and projected the STP onto the PD array. In the radial direction, each STP column consists of several bell-shaped transmissive zones, through which the PD array is masked; thus, the PDs toward the ends of the transmissive zones were increasingly blocked. Consequently, the effective sensing area of the PD array peaked toward its middle and progressively reduced toward its ends.

The maximum height  $H$  and width  $P_1$  of each bell-shaped transmissive zone were selected such that a sinusoidal spatial distribution of the transmitted power occurred. The proposed design, which uses several small bell-shaped transmissive zones in a column, is suitable for a divergent LED source. Moreover,

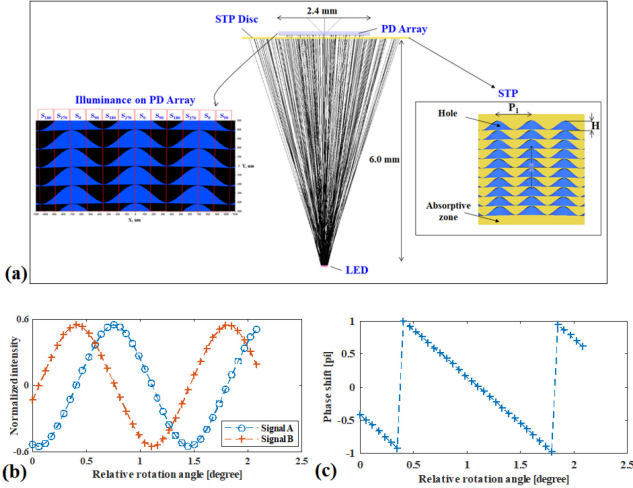


Fig. 5. (a) Designed rotary encoder with structural parameters shown; (b) Illuminance spatial distribution output obtained with LightTools; (c) Phase-shift calculation performed using the direct arctangent.

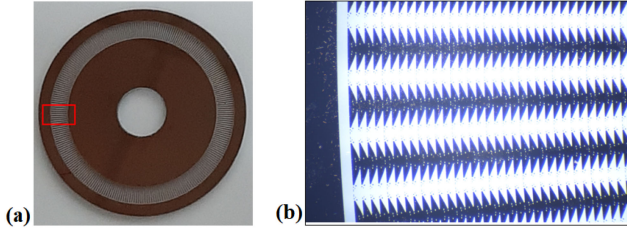


Fig. 6. (a) Columns of STP are arranged on the circumference (disc diameter: 60 mm); (b) Micrographs of the STP; each STP column is 688- $\mu\text{m}$  wide and 4000- $\mu\text{m}$  long.

our design has a high assembly tolerance and excellent performance.

For the designed disk, the output signals were estimated in terms of the rotation angle. As depicted in Fig. 5b, two sinusoidal signals simulated with the optical software LightTools [19], namely  $S_A$  and  $S_B$ , each with a period of 1.40625°, are acquired when the STP disk is rotated in the clockwise direction. The  $S_A$  signal leads the  $S_B$  signal by a phase equivalent to a quarter of the pitch. The  $S_B$  signal leads the  $S_A$  signal by the same phase when the STP disk rotates in the counterclockwise direction. As illustrated in Fig. 5c, one cycle of phase shift corresponds to the circumferential pitch  $P_1$ . Therefore, our design exhibits similar performance to that of a conventional rotary incremental encoder that uses an index grating imaged onto a scale grating.

### III. FABRICATION AND DISCUSSION

An STP disk was made of transparent glass covered with chrome patterns. Fig. 6a depicts a produced STP disk (diameter: 60 mm). Columns of STPs were arranged on the circumference of this disk. An enlarged micrograph of the red box in Fig. 6a is displayed in Fig. 6b. Each STP corresponded to a bell-shaped transmissive zone. To demonstrate the STP-based encoder, the transmitted sinusoidal signals currently are detected with a

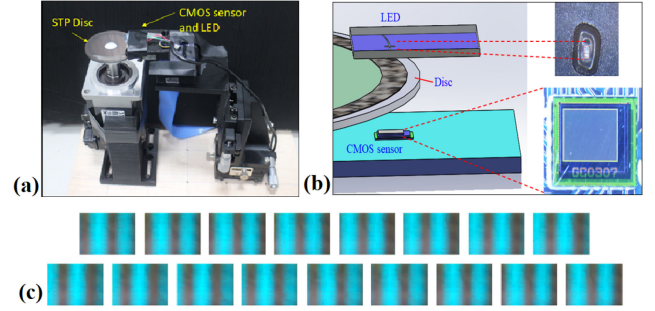


Fig. 7. Demonstration of the principle of the STP-based encoding pattern. (a) Optical setup; (b) Scheme of the light source and detection module; (c) STP images projected onto the CMOS image sensor at rotation angles from 0 to 1.73° in 17 steps.

CMOS camera. Replacing the PD array (four-phase quadrature detectors) with a camera as a detector is useful in the testing stage, since it allows us to initially clarify if the STP can perform well and its limitations. Norm conform measurements could not be conducted yet. Nevertheless, a verification of the basic functionality can be achieved. In the measurement, the encoder disk was attached on a PLC (programmable logic controller)-controlled motor. Fig. 7a illustrates the setup for demonstrating the working principle of the STP disk. The light source and detection module are displayed in Fig. 7b. The LED chip had a narrow emission peak centered at approximately 470 nm. The complementary metal oxide semiconductor (CMOS) image sensor had a size of 2 × 1.75 mm. The images were captured at a lower rotation speed, 60 rpm, which outputs the signals  $S_A$  and  $S_B$  with a frequency of 256 Hz for the STP line count of  $N = 256$ . A series of STP images is shown in Fig. 7c; these images represent the images projected onto the CMOS image sensor at rotation angles of 0 to 1.73° in 17 steps.

To obtain these images precisely, the shift between the STP disk and the sensing module has to be controlled well. If the STP encoder is not aligned on the correct position, it will distort the measured sinusoidal signals. As shown in Fig. 8a, if there is a tangential shift ( $\Delta X$ ), the PD array does not detect the measurement target at the correct pitch. Here a constant shift error ( $\Delta\theta$ ) occurs between the ideal assembly and the tangential shift. Our simulation shows that under a common assembly situation, if the  $\Delta X$  is 0.5 mm,  $\Delta\theta$  can be as high as 0.383°. As shown in Fig. 8b and 8c, when a radial shift ( $\Delta Y$ ) or a tilt ( $\Delta T$ ) of the disk occurs, the constant shift error ( $\Delta\theta$ ) under these two cases is very small. Simulations show that if the  $\Delta Y$  and  $\Delta T$  are 0.4 mm and 1.5°,  $\Delta\theta$  can be as low as 0.002° and 0.0012° respectively. However, as the assembly errors do not change with time, it is possible to compensate for this using the integrated signal correction facility. Phase-shift calculation results from these assembly errors are shown in Fig. 8d.

During assembly, the relative positions of the LED and CMOS image sensor were tuned by checking the image without the STP disk to minimize the assembly error. The CMOS image sensing data were divided into four zones to obtain the digital quadrature encoded signals  $S_A$  and  $S_B$  (Fig. 9a). With these two signals, the relative displacement produced between the STP disk and

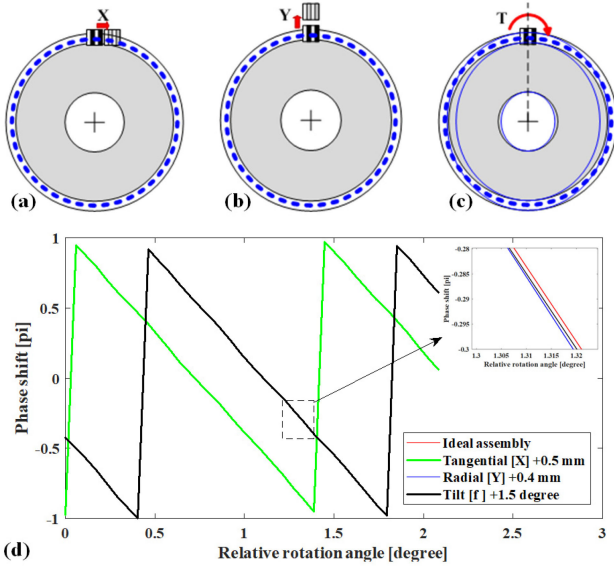


Fig. 8. Schematic diagram showing the conditions of (a) the tangential shift, (b) the radial shift, and (c) the tilt of disk. (d) Phase-shift calculation results of these assembly error conditions.

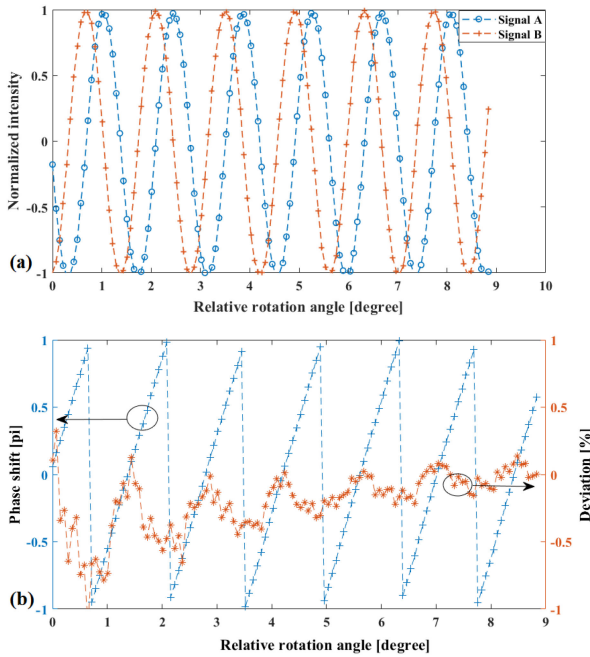


Fig. 9. (a) Spatial distribution of the illuminance output calculated from the measured data; (b) Phase-shift calculation performed using the direct arctangent and its deviation from the ideal condition.

the CMOS image sensor could easily be determined using Eq. (3), which presents the arctangent algorithm of the quotient between both signals (Fig. 9b). The result shows that the deviation from the ideal phase was within 0.5% and  $-1\%$ , which indicates that the signals could be processed with at least a 7-fold interpolation. As analyzed in the simulation, the deviation was mainly due to the pattern difference between the designed STP and the fabricated STP. Diffraction induced by the holes and edges of the STP makes some power of the transmitted

TABLE I  
COMPARISON BETWEEN THE PROPOSED ENCODER AND PRIOR ART

Reference	Encoder type	Feature	Outcome
Proposed encoder	Optical encoder (STR type)	Angular information has been sensed from bell-shaped sinusoidal transmissive patterns by an imaging sensor.	Available resolutions:15 bits
[7]	Optical encoder (diffractive type)	Angular information has been sensed from a diffractive solid measure on a microstructured plastic disk by an imaging sensor.	Available resolutions:15 bits
[11]	Optical encoder (polarization type)	Angular information has been achieved from the differential light intensity of the orthogonal polarization components.	Stable differential signal matching the theoretical Malus' law was obtained.
[12]	Optical encoder (ratio-metric type)	Angular information is determined by the ratio of the transmitted and reflected light powers.	The accuracy is 0.53% over the full range of $0^\circ$ to $180^\circ$ .
[14]	Optical encoder (binary type)	Angular information is determined from lines and windows printed in a transparent disk.	Maximal available resolutions via interpolation:22 bits
[20]	Magnetic encoder (13-bit magnetic Hall-effect)	Angular information is calculated from AC signals provided by Hall effect devices, which is actuated by a two-pole magnet mounted on the end of a shaft.	Available resolutions with accuracy to $\pm 0.3^\circ$ : 13 bits

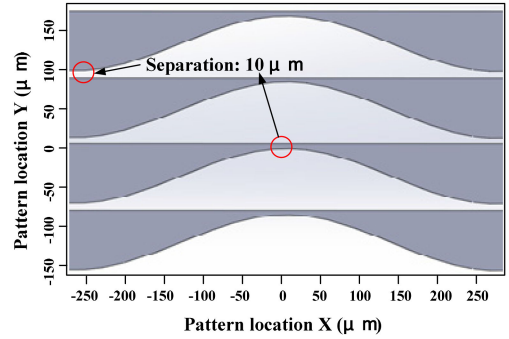


Fig. 10. STP in a continuous form.  $10\mu\text{m}$ -separation between the STPs along the radial direction are marked with red circles.

beam diffract onto the wrong region of the CMOS. The binary resolution, added with the designed 256 increments, amounts to 15 bit for the test setup. A comparison of our sensor with other types of incremental encoders is summarized in Table I. Our STP encoder offer high resolution. Like most optical encoders, they are fairly immune to electromagnetic interference but are susceptible to contamination, while the magnetic encoders are susceptible to electromagnetic interference unless properly shielded and provide lower resolution.

In addition to the assembly error, the measurement deviation can be attributed to the fabrication limit and the induced diffraction effect. The fabrication limit is from the limitation of linewidth of encoder pattern. In designing the STP, one constraint is the minimum pattern size and space has to be larger than  $4\mu\text{m}$ , which is limited by the local mask fabrication tool. Therefore, there is a deviation in the transmissive area between the fabricated and the ideal STP, as shown in Fig. 2b. These smaller pattern sizes and spaces further introduce diffraction and hence the intensity distribution through the fabricated STP onto the PD array will be different from that through the ideal STP.

More accurate sensing is possible by designing the fabricated STP in a continuous form (as shown in Fig. 10), which uses no small pattern sizes and spaces.  $10\mu\text{m}$ -separations are inserted between the STPs along the radial direction. This separation is large enough to reduce diffraction effect. Besides the separation induces no offset to the signals  $S_A$  and  $S_B$ .

#### IV. CONCLUSION

This paper describes the design and fabrication of an STP-based rotary encoder, which is used to decode angular displacement. The prototype comprises 256 columns of STPs to provide a detection pitch of  $1.40625^\circ$ . Higher resolution can be achieved via phase-shift interpolation. Each column comprises 50 bell-shaped transmissive patterns. The proposed STP encoder is an alternative encoder that can achieve the same angular resolution as a conventional geometric rotary encoder.

#### REFERENCES

- [1] V. Liberali, F. Cherchi, L. Disingrini, M. Gottardi, S. Gregori, and G. Torelli, "A digital self-calibration circuit for absolute optical rotary encoder microsystems," *IEEE Trans. Instrum. Meas.*, vol. 52, no. 1, pp. 149–157, Feb. 2003, doi: [10.1109/TIM.2003.809499](https://doi.org/10.1109/TIM.2003.809499).
- [2] K. Tobita, T. Ohira, M. Kajitani, C. Kanamori, M. Shimojo, and A. Ming, "A rotary encoder based on magneto-optical storage," *IEEE/ASME Trans. Mechatron.*, vol. 10, no. 1, pp. 87–97, Mar. 2005, doi: [10.1109/TMECH.2004.842230](https://doi.org/10.1109/TMECH.2004.842230).
- [3] S.-H. Jeong, S. Rhyu, and B.-I. Kwon, "Design of the rotary magnetic position sensor with the sinusoidally magnetized permanent magnet," in *Proc. 12th Biennial IEEE Conf. Electromagn. Field Computation*, 2006, pp. 243–243, doi: [10.1109/CEFC-06.2006.1633033](https://doi.org/10.1109/CEFC-06.2006.1633033).
- [4] V. A. Tarkov, "Construction features of positional angle sensors of modern geodesic devices," *J. Opt. Technol.*, vol. 78, no. 5, pp. 336–340, 2011, doi: [10.1364/JOT.78.000336](https://doi.org/10.1364/JOT.78.000336).
- [5] T. Wigmore, "Optical shaft encoder from sharp," *Elektor Electron*, vol. 15, no. 169, pp. 60–62, 1989.
- [6] V. Mayer, T. Botzelmann, K. P. Fritz, J. Seybold, and H. Kück, "A new concept for an absolutely encoded angular resolver," in *Proc. 4M 2007 Conf. Multi-Mater. Micro Manufacture*, 2007, pp. 3–5.
- [7] D. Hopp *et al.*, "Diffraction incremental and absolute coding principle for optical rotary sensors," *Appl. Opt.*, vol. 50, no. 26, pp. 5169–5177, Sep. 2011, doi: [10.1364/AO.50.005169](https://doi.org/10.1364/AO.50.005169).
- [8] Y. C. Chen, C. H. Lee, M. J. Chou, and S. Shen, "High-precision digital rotary encoder based on dot-matrix gratings," *IEEE Photon. J.*, vol. 10, no. 2, pp. 1–12, Apr. 2018, doi: [10.1109/JPHOT.2017.2781465](https://doi.org/10.1109/JPHOT.2017.2781465).
- [9] S. Makinouchi, A. Watanabe, M. Takasaki, T. Ohara, J. H. Ong, and S. Wakui, "An evaluation of a modulated laser encoder," *Precis. Eng.*, vol. 35, no. 2, pp. 302–308, Apr. 2011, doi: [10.1016/j.precisioneng.2010.11.008](https://doi.org/10.1016/j.precisioneng.2010.11.008).
- [10] D. Chang, X. Xing, P. Hu, J. Wang, and J. Tan, "Double-diffracted spatially separated heterodyne grating interferometer and analysis on its alignment tolerance," *Appl. Sci.*, vol. 9, no. 2, 2019, Art. no. 263, doi: [10.3390/app9020263](https://doi.org/10.3390/app9020263).
- [11] S. Ikeda, E. Higurashi, T. Suga, and T. Oguchi, "Miniaturized polarization sensors integrated with wire-grid polarizers," in *Proc. Int. Conf. Electron. Packag.*, 2014, pp. 376–379, doi: [10.1109/ICEP.2014.6826712](https://doi.org/10.1109/ICEP.2014.6826712).
- [12] T. A. Tameh, M. Sawan, and R. Kashyap, "Novel analog ratio-metric optical rotary encoder for avionic applications," *IEEE Sensors J.*, vol. 16, no. 17, pp. 6586–6595, 2016, doi: [10.1109/JSEN.2016.2588981](https://doi.org/10.1109/JSEN.2016.2588981).
- [13] J. Slack and R. J. Bale, "Encoder apparatus that includes a scale and a readhead that are movable relative to each other configured to reduce the adverse effect of undesirable frequencies in the scale signal to reduce the encoder sub-divisional error," U.S. patent 10,670,431B2, Jun. 2020.
- [14] "EncodersBlue goes reflective," [Online]. Available: [https://www.ichaus.de/upload/pdf/iC-Haus-Reflective-encoder-iCs\\_whitepaper\\_A1en.pdf](https://www.ichaus.de/upload/pdf/iC-Haus-Reflective-encoder-iCs_whitepaper_A1en.pdf)
- [15] M. R. Wang and H. Su, "Laser direct-write gray-level mask and one-step etching for diffractive microlens fabrication," *Appl. Opt.*, vol. 37, pp. 7568–7576, 1998.
- [16] W. Henke, W. Hoppe, H. J. Quenzer, P. Staudt-Fischbach, and B. Wagner, "Simulation and experimental study of gray-tone lithography for the fabrication of arbitrarily shaped surfaces," in *Proc. IEEE Micro Electro Mech. Syst. An Investigation Micro Structures, Sensors, Actuators, Mach. Robotic Syst.*, 1994, pp. 205–210.
- [17] S. H. Kim, S.-H. Lee, and C. C. Chung, "Phase shift calibration method in optical sinusoidal encoder signals applied to servo track writer," *IFAC-PapersOnLine*, vol. 49, no. 21, pp. 1–6, 2016, doi: [10.1016/j.ifacol.2016.10.502](https://doi.org/10.1016/j.ifacol.2016.10.502).
- [18] Interface to Sin/Cos Encoder With Sitara AM437x (Rev. A) (ti.com). [Online]. Available: [https://www.ti.com/lit/ug/tidua77a/tidua77a.pdf?ts=1615697813263&ref\\_url=https%253A%252F%252Fwww.bing.com%252F](https://www.ti.com/lit/ug/tidua77a/tidua77a.pdf?ts=1615697813263&ref_url=https%253A%252F%252Fwww.bing.com%252F)
- [19] LightTools Software. [Online]. Available: <https://www.synopsys.com/optical-solutions/lighttools.html>
- [20] Rotary Magnetic Shaft Encoder, RE36. [Online]. Available: <https://www.rls.si/eng/re36-rotary-magnetic-shaft-encoder#product-datasheet-data>